HHS Public Access

Author manuscript

J Mol Biol. Author manuscript; available in PMC 2022 September 17.

Published in final edited form as:

J Mol Biol. 2021 September 17; 433(19): 167178. doi:10.1016/j.jmb.2021.167178.

Interaction of the C2 Ig-like Domain of Cardiac Myosin Binding Protein-C with F-actin

Cristina M. Risi[1], **Malay Patra**[1], **Betty Belknap**[1], **Samantha P. Harris**[2], **Howard D. White**[1], **Vitold E. Galkin**[1,*]

[1]Department of Physiological Sciences, Eastern Virginia Medical School, Norfolk, VA 23507, USA

[2]Department of Cellular and Molecular Medicine, University of Arizona, Tucson, AZ 85724, USA

Abstract

Cardiac muscle contraction depends on interactions between thick (myosin) and thin (actin) filaments (TFs). TFs are regulated by intracellular Ca^{2+} levels. Under activating conditions Ca^{2+} binds to the troponin complex and displaces tropomyosin from myosin binding sites on the TF surface to allow actomyosin interactions. Recent studies have shown that in addition to Ca^{2+}, the first four N-terminal domains (NTDs) of cardiac myosin binding protein C (cMyBP-C) (e.g. C0, C1, M and C2), are potent modulators of the TF activity, but the mechanism of their collective action is poorly understood. Previously, we showed that C1 activates the TF at low Ca^{2+} and C0 stabilizes binding of C1 to the TF, but the ability of C2 to bind and/or affect the TF remains unknown. Here we obtained 7.5 Å resolution cryo-EM reconstruction of C2-decorated actin filaments to demonstrate that C2 binds to actin in a single structural mode that does not activate the TF unlike the polymorphic binding of C0 and C1 to actin. Comparison of amino acid sequences of C2 with either C0 or C1 shows low levels of identity between the residues involved in interactions with the TF but high levels of conservation for residues involved in Ig fold stabilization. This provides a structural basis for strikingly different interactions of structurally homologous C0, C1 and C2 with the TF. Our detailed analysis of the interaction of C2 with the

*Correspondence should be addressed to: V.E.G., Department of Physiological Sciences, Eastern Virginia Medical School 700 West Olney Road, Lewis Hall, Room 3126, Norfolk, VA 23507, galkinve@evms.edu, Tel: 1-757-446-5668.

Author contributions: C.M.R. performed image analysis, 3D-reconstructions, flexible fitting and model refinement, and wrote the manuscript, M.P. assisted C.R., B. B. purified proteins and ran enzyme kinetic assays, H.D.W. analyzed enzyme kinetic assays, S.P.H. contributed to experimental design and edited the manuscript, V.E.G. conducted cryo-EM, performed image analysis and 3D-reconstructions, and wrote the manuscript.

CRediT author statement

Cristina M. Risi: Investigation, Data Curation, Formal analysis, Visualization. **Malay Patra**: Investigation, Data Curation. **Betty Belknap**: Investigation, Data Curation, Formal analysis, Visualization. **Samantha P. Harris**: Methodology, Validation, Supervision, Writing - Review & Editing, Funding acquisition. **Howard D. White**: Methodology, Validation, Supervision, Writing - Review & Editing, Funding acquisition. **Vitold E. Galkin**: Conceptualization, Methodology, Validation, Supervision, Writing - Original Draft, Writing - Review & Editing, Project administration, Funding acquisition.

Declaration of Interests: The authors declare no competing interests.

Declaration of interests

The authors declare that they have no known competing financial interests or personal relationships that could have appeared to influence the work reported in this paper.

actin filament provides crucial information required to model the collective action of cMyBP-C NTDs on the cardiac TF.

Graphical Abstract

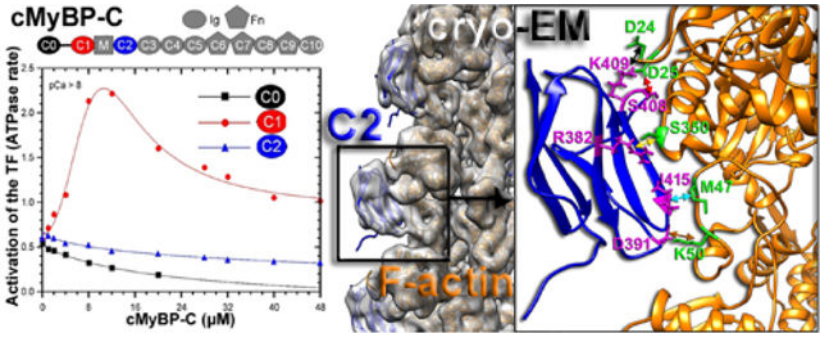

Keywords

thin filament; cardiac myosin binding protein C; cryo-electron microscopy; cardiac contraction; actin

INTRODUCTION

Mutations in *MYBPC3,* the gene encoding the thick filament accessory protein cardiac myosin binding protein C (cMyBP-C), are one of the leading causes of hypertrophic cardiomyopathy (HCM), a disease affecting approximately 1 in 200 people [1]. Not surprisingly, there has been increasing attention given to understanding the role of cMyBP-C in regulating cardiac contraction and how mutations in *MYBPC3* cause disease. However, determining exactly how cMyBP-C affects the cycle of cardiac contraction and relaxation has proven challenging in part because, aside from its interactions with myosin-based thick filaments, cMyBP-C also interacts with thin filaments (TFs), comprised of filamentous actin (F-actin), the troponin (Tn) complex, and tropomyosin (Tm).

Two central functions for cMyBP-C have emerged so far. First, cMyBP-C appears to stabilize myosin heads in a folded back configuration on relaxed thick filaments [2] where the folded conformation promotes the super relaxed (SRX) state of myosin [3, 4]. Because myosin in the SRX state has an extremely low ATPase rate [5], by stabilizing myosin heads against the thick filament backbone cMyBP-C is thought to contribute to cardiac energetics as well as myosin activation and relaxation kinetics [6]. Consistent with this, HCM mutations in cMyBP-C have been identified that disrupt the SRX state [7]. Second, through its interactions with thin filaments cMyBP-C can directly modulate the activation state of the thin filament either by shifting tropomyosin to its “on” state or by competing with myosin heads [8–10]. Thus, through interactions with the thin filament cMyBP-C can further affect the extent, timing, and duration of thin filament activation and cross-bridge kinetics. For example, an HCM mutation was identified that increased both the binding affinity of cMyBP-C for actin and its ability to shift tropomyosin further towards its “on” state [11] leading to prolonged ejection time and slowed relaxation in transgenic mice with

this mutation [12]. Finally, the ability of cMyBP-C to interact with both myosin (thick) and actin (thin) filaments in muscle sarcomeres [13, 14] has led to the idea that cMyBP-C is important for communicating the activation state of each filament system to the other [15].

As shown in Figure 1, cMyBP-C is composed of eight Ig-like and three fibronectin (Fn)-like domains and a regulatory M-domain located between the C1 and C2 Ig domains (Figure 1(a)). The C0 Ig-domain at its N terminus is also connected to the C1 domain via a proline/alanine-rich linker (PA). The M-domain contains three canonical protein kinase A (PKA) phosphorylation sites at residues Ser275, Ser284, and Ser304 (human numbering) that are located within the disordered part of the M-domain [16]. A fourth site was also reported in cMyBP-C from mouse and humans [17], but the different sites are phosphorylated in a hierarchical manner and their usage differs according to kinase [18, 19].

Various experimental approaches have collectively demonstrated that fragments containing the N terminal domains (NTDs) of cMyCP-C (e.g. C0, C1, M, and C2) can bind F-actin [8, 10, 13, 20–24]. It has also been recognized that the specific regions of interaction may be isoform- and species-dependent with differences reported between cardiac and skeletal MyBP-C proteins and human versus mouse [22, 25]. Neutron scattering data suggested that C0 and C1 bind near subdomain 1 (SD1) of actin [20], which was subsequently confirmed by 3D reconstruction of negatively stained C0- and C1-decorated actin filaments [23]. 3D reconstructions of negatively stained TFs further revealed that binding of cMyBP-C to TFs shifts Tm to the high Ca^{2+} structural state [26], thus accounting for the activating effects of cMyBP-C NTDs reported by numerous groups [27–29]. However, in those studies the position of the bound domains were not resolved. A later study employed cryo-EM to visualize C0 and C1 bound to the TF [10] and to show that the two Ig domains bind polymorphically to actin (e.g. they interact with multiple sites on the actin molecule). Moreover, C0 was found to not activate the TF, while C1 activated the TF in a concentration dependent manner even in the absence of Ca^{2+} [10]. Subsequent studies showed that C1 can activate the TF through a direct interaction with Tm via a positively charged RASK loop (residues R215-K218), while the cardiac specific C0 domain contributes to C1-induced TF activation by enhancing C1 binding to the TF [24]. The regulatory M domain has also been shown to bind to the TF in a phosphorylation dependent manner [30]. However, direct evidence for whether the last NTD (e.g. C2) binds to the TF has not yet been reported. Interestingly, all the three N-terminal Ig-like domains have being shown to interact with the myosin head. Specifically, C0 domain has been shown to bind to the myosin regulatory light chain (RLC) [31], while C1 and C2 were found to interact with myosin S2 [32, 33].

Interactions of the cMyBP-C with the TF and myosin heads are regulated in part by phosphorylation of the M-domain depending on Ca^{2+}. Phosphorylation of the M domain at low Ca^{2+} has been shown to induce compaction of the NTDs (e.g. C0-C1-M-C2) which reduces its interactions with the TF [34, 35]. At the same time phosphorylation of the M domain reduces the ability of cMyBP-C to bind to myosin S2 and inhibit the thick filament [36][19]. However, formulating a more complete picture of how cMyBP-C NTDs regulate the activation state of thick and thin filaments is hindered by the lack of structural data on the interactions of the M and C2 domains with the TF. Therefore, the goal of this study was to use a combined approach of cryo-EM and biochemical kinetics to identify

the interaction of the C2 Ig-like domain of human cMyBP-C with cardiac actin filaments. Results demonstrate that C2 binds to F-actin in a single structural mode, which differentiates C2 binding from the pattern of polymorphic binding typical of C0 and C1 binding to F-actin. We also show that C2 does not activate the TF.

RESULTS

The C2 Domain of cMyBP-C inhibits but does not activate cardiac thin filaments.

Previously, we have shown that C1 but not C0 activates the TF at low Ca^{2+} levels [10, 24]. To reveal if C2 is sufficient to activate or inhibit the cTF we used a steady state ATPase assay to measure the effect of C2 on the TF-activated rates of myosin-subfragment 1 (myosin-S1) ATP hydrolysis and compared it to effects of C0 and C1. As shown in Fig. 1(b), C0 and C2, have dramatically different effects on TF activation at low Ca^{2+} (pCa>8) in comparison to C1. C1 exerts a concentration-dependent biphasic effect on the activation state of the TF with maximal activation at ~10 μM (Figure 1(b) red curve). We have demonstrated previously [2, 5] that C1 binds to multiple sites on the surface of the TF, so that in a “side” binding mode it activates the TF, while in a “front” binding mode it competes with myosin-S1 for binding to the TF. Therefore, at higher concentrations of C1, despite its activation effect on the TF, it likely competes with myosin-S1 for binding to the TF thus accounting for its inhibitory effects on the TF-activated myosin-S1 ATPase rates. However, in contrast to C1, both C0 (Figure 1(b), black curve) and C2 (Fig. 1(b), blue curve) do not activate the TF, but rather inhibit it in a concentration dependent fashion. Interestingly, C2 appears less effective than C0 at inhibiting TF-dependent myosin-S1 ATP hydrolysis than C0. Because C2 lacks an activating effect on ATPase activity, we conclude that it should also not interfere with the Tm position on the surface of the cTF.

The structure of C2 decorated cardiac F-actin.

Next, we sought to determine whether C2 binds to the cTF, and if so, where it binds on the surface of F-actin. In our previous studies [10, 24] we used cTFs decorated with either C0 or C1. However, helical averaging of C0/C1 with the Tn complex components limited the resolution of reconstructions from those studies to moderate ~11 – 15 Å. Considering that C2 does not activate the cTF (Fig. 1(b), and that the presence of Tn complex leads to reduced resolution, for structural analysis we used F-actin instead of cTF. We performed 3D reconstructions of frozen hydrated cardiac actin filaments decorated with the C2 utilizing a single particle approach [33] (Fig. S1). The overall 3D reconstruction of C2-decorated F-actin showed traces of C2 bound to the front of F-actin (Fig. S1(b), red arrows) suggesting that F-actin was only partially decorated with C2. To obtain better details of C2 bound to F-actin we sorted C2-F-actin segments into bare, partially decorated, and fully decorated classes (Fig. S1(c–e)). Consistent with the low C2 density in the overall reconstruction, sorting revealed that only ~16% of the dataset represented F-actin segments extensively decorated with C2 (Figure S1(d)). Those fully decorated segments were therefore used to calculate the final 3D density map, which is shown in Fig. 2(a). The 6.1 Å resolution of the map (using FSC 0.143 criterion as shown in Fig. S2(a)) was not uniform - while the F-actin structure yielded a great match with the model of the actin filament at 6.1 Å resolution (PDB: 3MFP) [47] (Fig. S2(c)), the C2 density gave a good match with the C2 NMR

structure (PDB: 1PD6) only at 7.5 Å resolution (Fig. S2(d)). The pseudo-atomic model refinement (Fig. S1(d)) introduced minimal perturbations into the actin and C2 structures (Fig. S2(e)). As expected, the use of F-actin instead of cTF significantly improved the resolution.

We next analyzed the interface between the C2 and actin to predict possible contacts that hold C2 on the surface of F-actin (Fig. 2(b)). We found that the negatively charged D24 and D25 residues of actin are in proximity to K409 and S408 of C2 suggesting that D24 forms a salt bridge with the K409 (Fig. 2(c), black arrow), while D25 makes and H-bond with the S408 (Fig. 2(c), red arrow). C2 R382 may also form an H-bond with S350 of actin (Fig. 2(c), yellow arrow), while C2 I415 is likely to make a hydrophobic interaction with M47 of actin (Figure 2(c), cyan arrow). Finally, a salt bridge between C2 D391 and K50 of actin (Figure 2(c), brown arrow) presumably connects the lower loop of C2 to F-actin.

To exclude the possibility that low occupancy versus fully decorated segments represent different modes of C2 binding to the actin filament, we next compared the two classes at 10 Å and 15 Å resolutions (Fig. S3(a) and (b), respectively). While there was a difference in the size of the C2 density between the fully and partially decorated maps at 10 Å resolution (Fig. S3(a)), this difference was nearly eliminated at a higher 15 Å resolution (Fig. S3(b)). Since the model for the C2-F-actin complex yielded a perfect fit into the15 Å resolution map (Fig. S3(b), red arrow), the main difference between the two aforementioned structural classes was occupancy, rather than the positioning of the C2 on the surface of the actin filament.

Prediction of C2 interactions with the cTF.

To determine how C2 may bind to actin subunits in the context of the complete cTF, we next superimposed the map and the atomic model of the C2 decorated F-actin complex onto the recently published model of the cTF in the Ca^{2+}-free (Fig. 3(a)) and Ca^{2+}-bound (Fig. 3(c)) states [37]. Results showed that binding of C2 may be sensitive to the to Ca^{2+}-bound state of the cTF because under Ca^{2+}-free conditions only three (e.g. subunits 2, 3 and 6 numbered in green in Fig. 3(a)) out of six actin subunits forming a backbone of the regulatory unit were permissive for interactions with C2. Subunit 1 had the TnT N-terminal segment clashing with C2 (Fig. 3(b), cyan arrow), while subunit 5 showed a severe clash with the TnI C-terminal extension (Fig. 3(d), magenta arrow). Under both Ca^{2+}-free and Ca^{2+}-bound TF states subunit 4 was not available for C2 binding due to a steric clash of C2 with the core of the Tn complex (Fig. 3(a) and (c), black arrows). C2 positioning on F-actin was also not compatible with simultaneous myosin-S1 binding (Fig. 3(e), red arrows). The latter may explain the concentration-dependent inhibition of cTF actomyosin interactions by C2 (Fig. 1(b)). Interestingly, these data predict that C2 may bind better to the Ca^{2+}-bound cTF, since there are 5 actin subunits available for C2 binding under these conditions (Fig. 3(c), green numbers) compared to only 3 subunits available for C2 binding under Ca^{2+}-free conditions (Fig. 3(a), green numbers). To test this prediction we performed additional cosedimentation binding assays using either F-actin or cTFs at low (pCa>8) and high (pCa<4) Ca^{2+} concentrations (Fig. 4). Results showed that consistent with predictions from structural modeling, C2 bound to F-actin at a higher apparent stoichiometry (0.73 ±

0.11 C2 per actin) than to the cTF at either low Ca^{2+} (0.58 ± 0.3 C2 per actin) or high Ca^{2+} (0.33 ± 0.07 C2 per actin). Binding affinity of C2 for F-actin (K_d = 24.0 ± 7.6 μM) was similar to that previously determined for C0 (K_d = 17.8 ± 3 μM) [10]. However, the binding affinity of C2 for cTF at high Ca^{2+} levels (K_d = 14.8 ± 7.5 μM) was significantly greater than at low Ca^{2+} (K_d = 56.4 ± 45.4 μM), consistent with predictions from structural models indicating that C2 should have fewer barriers to binding at high Ca^{2+} concentrations relative to low. The weaker binding affinity measured for C2 at low Ca^{2+} levels relative to that of C0 (K_d = 13.4 ± 4 μM) [10] is also consistent with weaker inhibition of the rate of TF-dependent myosin-S1 ATP hydrolysis by C2 in comparison to C0 (Fig. 1(b)).

However, note that the relatively low affinity of C2 for cTF at pCa>8 gave rise to variablilty in experimental measurements resulting in high standard deviations, presumably because all experimental points tested were below the apparent K_d. Attempts to use higher C2 concentrations to reduce variability were not successful (not shown) possibly due to the small fraction of C2 bound to cTFs. Thus, results from cosedimentation experiments were generally consistent with predictions from structural analyses suggesting a weaker interaction of C2 with the cTF at low Ca^{2+}, but were not robust enough to unambiguously support structural predictions at this time.

Comparison of C0, C1 and C2 interface on F-actin.

Next, we compared binding modes of C2 with F-actin to that of C0 and C1. Results shown in Figure 5 demonstrate that while C0, C1 and C2 domains are all structural homologues of one another (i.e., they all belong to the same Ig-like family of proteins), they all bind to cTF actin subunits in different modes (Fig. 5). C0 thus binds to the front of the actin molecule in two discrete modes (e.g., mode 1 and mode 2), related by ~125° in-plane rotation [10] (Fig. 5(a) and (b), cyan ribbons for modes 1 and 2, respectively). When present in tandem, C0 and C1 also have two preferred modes of binding, each having C0 first bound to the front of the TF (in either mode1 or mode 2), and C1 bound exclusively to the side of the TF bridging actin with the Tm cable (Fig. 5(a) and (b), C1 is shown as red ribbons) [24]. However, it is notable that both modes of C0 binding are thus predicted to overlap with C2 bound to F-actin (Fig. 5(a) and (b), red arrows). Nevertheless, the interface of C0 and C1 with F-actin is still distinguishable because in contrast to either of the two C0 binding modes, C2 interacts with not one, but two actin subunits simultaneously including the actin protomer immediately below C2 (Fig. 5(a) and (b), red ovals). Due to relatively low resolution of the C0–C1 decorated cTF cryo-EM maps (i.e. ~11 Å) [24] it was not possible to directly compare the C0 and C2 interfaces on F-actin. Nevertheless, we determined whether the C2 residues involved in the interactions with F-actin are conserved between the three Ig-like domains (Fig. 5(c–e)). First we compared the NMR structure of the C0 domain (PDB: 2K1M) with C2 from our C2-F-actin model (Fig. 5(c), grey and blue ribbons, respectively). We plotted the outcome of the CLUSTAL alignment of the C0 and C2 sequences (Fig. 5(e)) onto their structures (Fig. 5(c), grey and blue, respectively) to determine the positioning of conserved amino acids (Fig. 5(c), marked green). The sequence alignment revealed a 27.8% identity and 45.4% similarity between C0 and C2. Not surprisingly, the conserved sequences between C0 and C2 were mostly positioned within the β-strands that comprise the Ig-like domain fold (Figure 5(c), green ribbons), while only one out of five C2 residues involved

in the interactions with F-actin was conserved between C0 (K54) and C2 (K409) (Fig. 5(c), black arrows, and (e), green ovals). Similar comparisons between C2 and C1 (Fig. 2(d), grey and blue ribbons, respectively) revealed a 23.1% identity and 35.0% similarity between the C1 and C2 domains with most of the conserved residues located in the β-strands (Fig. 5(d), green ribbons). Again, only one out of five amino acids involved in C2 interactions with F-actin (Fig. 5(d), black arrows, and (e), green ovals) was conserved between C1 (H206) and C2 (K409). Both K54 of C0 and H206 of C1 were proposed to be involved in interactions with the cTF, but those interactions are very different from the contacts that C2 makes with the actin subunits [10].

Comparison of residues predicted to facilitate binding of cardiac C1 and C2 to the TF between cardiac and skeletal MyBP-C isoforms.

To better understand the role of individual N-terminal Ig-like domains (e.g. C1 and C2) in TF activation we compared the conservation of the TF binding sites between the three isoforms of MyBP-C (e.g. fast-skeletal, slow-skeletal, and cardiac). The CLUSTAL alignment of cardiac C1 and slow skeletal C1 indicated 52.9% identity (69.4% similarity), while the cardiac C1 and fast skeletal C1 revealed only 39.3% identity (51.4% similarity). The comparison of cardiac C1 residues predicted to be involved in the interactions with the TF [10, 24] with those form the slow and fast skeletal C1 isoforms (Fig. 6(a), red boxes) showed that the slow isoform possessed ~69% similarity with the cardiac isoform in abovementioned regions, while the fast skeletal isoform showed 57% similarity. The most striking difference between the slow and fast isoforms when compared with the cardiac isoform was found in the "RASK" loop involved in the cardiac TF activation [24] – similar to the cardiac isoform, the slow skeletal isoform contained two positively charged residues (RHSR), while the fast skeletal isoform had those residues replaced with neutral amino acids (SASN). Consistent with these residues being involved in TF activation, it was shown that while N-terminal domains of the cardiac and the slow skeletal isoforms were capable of shifting the tropomyosin cable away from the myosin binding sites on the TF at low Ca^{2+} levels (pCa=9), the fast skeletal isoform was not capable of activating the TF at low Ca^{2+} levels [38]. Therefore, conservation of positively charged residues in the cardiac (RASK) and slow skeletal (RHSR) isoforms are important for TF activation.

A CLUSTAL alignment of cardiac and slow skeletal C2 revealed 59.6% identity (70.2% similarity), while the cardiac and fast skeletal C2 alignment showed 63.8% identity (80.9% similarity) (Fig. 6(b)). The positively charged K409 in the cardiac isoform (Fig. 6 (b), black arrow), which makes salt bridge with D24 of actin (Fig. 2(c), black arrow), is conserved in fast skeletal (K301) and slow skeletal (K297) isoforms. Cardiac polar uncharged S408 (Fig. 6 (b), red arrow) is predicted to form an H-bond with D25 of actin (Fig. 2(c), red arrow), and is conserved in the fast skeletal (S300). In the slow skeletal isoform this residue is substituted with conserved T296. The cardiac positively charged R382 (Fig. 6 (b), yellow arrow), which presumably forms an H-bond with S350 of actin (Fig. 2(c), yellow arrow), is also conserved between the fast (K275) and slow (R271) skeletal isoforms. The non-polar I415 (Fig. 6 (b), cyan arrow) that may form hydrophobic interactions with M47 of actin (Fig. 2(c), cyan arrow) in cardiac C2 is replaced with a hydrophobic residue (V307) in the fast skeletal isoform, while in the slow skeletal isoform this position has non-identical positively

charged K303. Another deviation in the actin binding residues between the three isoforms is observed at the negatively charged D391 in cardiac C2 (Fig. 6 (b), brown arrow), which is predicted to staple C2 to two adjacent actin subunits through a salt bridge with K50 (Fig. 2(c), brown arrow). Although, the fast skeletal C2 has identical a negatively charged residue (D284), the slow skeletal C2 contains a positively charged residue (K280). Therefore, in contrast to C1, C2 of the fast but not the slow skeletal isoform is predicted to have very similar interface on the surface of F-actin.

It has been shown that cMyBP-C activation of the TF is species dependent [25, 39]. Therefore, we also compared the sequences of human and murine C2 isoforms (Fig. S3). The alignment revealed 96.8% identity and 98.9% similarity between the two isoforms with only one conserved substitution I415 to V411 (Fig. S4, red arrow). Therefore, we do not anticipate any species-specific differences in interactions of C2 with the actin filament.

DISCUSSION

It has been previously shown that structurally homologous actin binding proteins may bind to F-actin in different modes. For example, calponin homology (CH) domain does not bind F-actin [40, 41], while in a protein such as fimbrin the CH3 and CH4 domains interact with F-actin in a very different fashion [42]. Here we show that the conserved sequences between C0 and C2 are mostly positioned within the β-strands that comprise the Ig-like domain fold (Figure 5(c), green ribbons). Similarly, comparisons between C2 and C1 (Fig. 2(d), grey and blue ribbons, respectively) reveals most of the conserved residues located in the β-strands (Fig. 5(d), green ribbons). Therefore, the structural conservation of the cMyBP-C Ig domains dictates elevated similarities between amino acids involved in the Ig fold stabilization, while low sequence similarity in the loops involved in the cTF interactions promotes divergence in the cMyBP-C NTDs binding to the cTF. Thus, while C0, C1, and C2 domains are structural homologs that bear high similarity to each other (Figure 5), homology alone does not imply their conserved functional interactions with actin.

The different patterns of binding of C0, C1 and C2 on the surface of F-actin are consistent with their distinct functional effects on actomyosin interactions and suggest that each domain evolved for a distinct purpose. All three C0, C1, and C2 domains have been shown to bind myosin heads [31–33], and prior to our study it was unknown whether C2 could bind to actin. Therefore, our data show that C2 like C0 and C1 can interact with actin and thus all three domains are capable of binding to both thin and thick filaments. The ability of these N-terminal domains may be important for dynamic interactions of cMyBP-C with both myosin and actin filaments [14, 43]. Our data suggests that C2 may bind with increased affinity to the activated cTF (Fig. 4). Taking in account that C1 can activate the TF in the absence of Ca^{2+}, and that C0 greatly enhances C1-dependent TF activation [24], it is plausible that C0 and C1 sequentially bind to the TF first to activate it at low Ca^{2+} levels, while C2 binds to already activated TF to lock the cMyBP-C NTDs on the surface of the cTF. This idea is supported by comparison of effects of C1-M and C1-M-C2 on the TF activation in skinned rat trabeculae, which showed that C2 increases the Ca^{2+}-sensitivity [9]. Recently, it has also been shown that C0-C1-M-C2-C3 fragment of cMyBP-C binding to the TF is a two-step process that involves initial weak binding followed by the tight bound

state [22]. Our data suggest that C2 may contribute to the transition from the weak to tight interaction with the TF.

MyBP-C is expressed is three isoforms: fast-skeletal, slow-skeletal, and cardiac. Despite the fact that the skeletal MyBP-C isoforms are conditionally coexpressed in cardiac muscle, it has been shown that the two skeletal isoforms are likely be tuned to meet the needs of specific skeletal muscles [38]. Comparison of residues predicted to facilitate binding of cardiac C1 and C2 to the TF between cardiac and skeletal MyBP-C isoforms (Fig. 6) reveals conservation of the positively charged residues in the cardiac (RASK) loop and slow skeletal (RHSR) that likely contribute to the ability of these two isoforms to activate the TF. However, the fast skeletal isoform has those positively charged residues substituted with neutral amino acids (SASN), and presumably because of this substitution it cannot activate the TF [38].

In contrast to C1, our data also predicts that cardiac C2 and fast skeletal C2 but not slow skeletal should have very similar interfaces on the surface of F-actin. Taken together, our data strongly suggest that the collective differences in the TF interacting residues of C1 and C2 domains between the three cMyBP-C isoforms should contribute to the tissue specific modulation of the TF by the N-terminal domains of MyBP-C.

MATERIALS AND METHODS

Isolation and Purification of cDNA

N-terminal cMyBP-C proteins containing the C0, C1, and C2 domains were cloned by PCR amplification of a full-length human cMyBP-C cDNA sequence (GenBankTM accession number NM000256) using upstream and downstream primers containing restriction site sequences for NdeI and HindIII, respectively. The resulting PCR products were cloned into the Zero-Bluntvector (Invitrogen #K2750) and gel-purified following NdeI/HindIII digestion. For expression in bacteria, gel-purified inserts were subcloned into the pQE-2 expression vector (Qiagen #32932) in frame with a His6-tag at the N terminus of the clone sequence to facilitate purification.

Protein Expression in E.coli

A 100 μl aliquot of competent M15[pREP4] cells (Qiagen #34210 – no longer commercially available) was thawed on ice. 2mg cDNA was added and flicked to mix. The mixture was left on ice for 20 minutes followed by heat shocking at 42°C for 90 seconds. 500ml of pre-warmed sterile Psi broth (10 ml LB broth without antibiotics, 4 mM $MgSO_4$, 10 mM KCl) was added to the cell/DNA mixture. This was incubated at 37°C and 230 rpm for 90 minutes. Aliquots of 10 and 25 ml were plated on LB Agar (1.5% (w/v) agar) containing 25 mg/ml kanamycin (in water) and 100mg/ml carbenicillin (in 20% (w/v) ethanol) (LB+K+C) followed by overnight incubation at 37°C. Several 5 ml LB+K+C were inoculated with single colonies and incubated by shaking at 230 rpm for 16 hours at 37°C. Following overnight incubation, the cells were pelleted by centrifugation at 3500 rpm for 10 minutes. The supernatants were removed and the pellets were re-suspended with 5 ml of fresh LB+K+C. Each re-suspended 5 ml culture was transferred to a 2 liter baffled flask

containing 500 ml of pre-warmed LB+K+C. The flasks were incubated at 37°C /200 rpm until the OD595 = 0.5 – 0.7. IPTG induction was done by using 1 mM IPTG. Then the temperature was quickly reduced to 30°C and the cultures were incubated for 6 hours at170 rpm. Cells from each culture were collected by centrifugation at 5500xg for 15 minutes. Supernatants were discarded and pellets were re-suspended in 10 ml of cold LB+K+C and transferred to 50 ml conical tubes. The transferred pellets were collected by centrifugation at 3,000xg for 10 minutes at 4°C. Supernatants were discarded and pellets were stored at −20°C.

Protein Purification

C2: A 5ml nickel-nitrilotriacetic acid (NiNTA: Qiagen #30210) was prepared for use by placing 10 ml of a 50% slurry of resin in a disposable column. The column was rinsed with 5 bed volumes of water before being equilibrated with 10 bed volumes of 2x Lysis Buffer (50 mM 2-Amino-2-(hydroxymethyl)propane-1,3-diol (TRIS), 400 mM NaCl, 30mM imidazole (pH 7.5)). The buffer was drained from the resin and the column was left at 4°C until needed. A frozen cell pellet containing the desired recombinant cMyBP-C was thawed on ice. The pellet was completely resuspended in cold Extraction Buffer (15 ml of Bacterial Protein Extraction Reagent (BPER), 100 ml HALT 2,2′,2″,2‴-(Ethane-1,2-diyldinitrilo)tetraacetic acid (EDTA)-free protease cocktail, 30 ml 1 mg/ml pepstatin-A in dimethyl sulfoxide (DMSO), 30 ml 100 mM PMSF, 30 ml 10 mM E64 protease inhibitor, 2.1 ml 2-mercaptoethanol and 1 complete Mini protease inhibitor tablet. The resuspended pellet was transferred to a 50ml conical centrifuge tube. 30 mg of lysozyme was added to the mixture and mixed gently. This was placed on a rotator at 50 rpm for 15 minutes at 4°C. After 15 minutes, 75 ml of 10,000 units/ml DNase (final concentration of 50 units per ml) was slowly added to the suspension. The tube was returned to the rotator for another 15 minutes. The suspension was diluted with an equal volume (15 ml) of 2X Lysis Buffer (50 mM TRIS (pH 7.5), 400 mM NaCl, 30 mM imidazole) before centrifugation at 25,000xg for 30 minutes at 4°C. The supernatant was used to resuspend the equilibrated NiNTA resin. The resuspended resin/lysate was placed in a 50 ml conical and placed on a rotator at 4°C/50 rpm for 75 minutes. The resuspended resin was removed from the rotator and poured into a 30ml disposable column and allowed to drain completely. 5ml aliquots of NiNTA Wash Buffer (25 mM TRIS (pH 7.5), 200 mM NaCl, 30 mM imidazole, 1 mM 2-mercaptoethanol, 0.1 mM phenylmethylsulfonyl fluoride (PMSF), 1 mg/ml pepstatin) were added and fractions were collected. Washing continued until the OD280 of the eluted fractions was less than 0.04. The column was then eluted by adding 1ml aliquots of NiNTA Elution Buffer (25mM TRIS (pH 7.5), 200mM NaCl, 250mM imidazole, 1mM 2-mercaptoethanol, 0.1mM PMSF, 1 mg/ml pepstatin) until the OD280 returned to baseline. The fractions eluted from the NiNTA column were run on a 15% polyacrylamide gel and appropriate fractions were pooled based on the presence of the desired protein and purity. Extinction coefficients and molecular weights for each construct were determined from their amino acid sequences using the ExPASy web tool. Concentrations were determined from the net OD280 after accounting for light scattering: Conc. (mg/ml) = (OD280 – (OD320 × 1.5))/extinction coefficient. The pooled fractions were concentrated and the buffer was exchanged using a 15 ml Millipore spin concentrating unit with a 10,000 MWCO. The final cMyPB-C samples deluted in 0.2 M potassium acetate (KAc), 10 mM 3-(N-morpholino)propanesulfonic acid

(MOPS), 3 mM $MgCl_2$ (pH 7.0) and were drip frozen and stored in liquid nitrogen until needed.

Actin: Cardiac actin was prepared from frozen rabbit hearts using the method of White and Siemankowski [44], which was a modification of the method of Spudich and Watt [45] for the preparation of actin from rabbit skeletal muscle.

Enzyme activity assay

cTF activation of steady-state ATP hydrolysis was measured as previously described [21] by a colorimetric assay in 50 mM KAc, 10 mM MOPS, 3 mM $MgCl_2$, 1 mM ATP, pH 7.0 in presence of 0.65 μM rabbit skeletal chymotryptic myosin-S1A1, 5 μM TF and indicated concentrations of cMyBP-C individual domains (e.g. C0, C1 and C2) and Ca^{2+} levels.

Cosedimentation assay

Spin down assays were done in the same buffer as used for ATPase measurements: 0.4 ml of solution containing 10 μM of either F-actin or TFs plus the indicated cMyBP-C C2 fragment concentration were centrifuged in 13 ml tubes in Beckman 70.1 rotor at 50,000 rpm (229,000 g) for 2 hours at 4° C. The supernatant was carefully removed and the concentration of C2 in the supernatant was determined by measuring optical density using the following formula: C = (A280 −1.5*A320) using an extinction coefficient of 0.00997 μM^{-1}. The amount of C2 bound to the cTF was determined by subtracting the concentration of C2 in the supernatant from its initial concentration.

Cryo EM Sample Preparation

[2 uM] of F-actin in 50 mM KAc, 10 mM MOPS, 3 mM $MgCl_2$, 2 mM EGTA (pCa>8), pH 7.0 were incubated with human C2 [15–20 uM] for 1–2 minutes. The suspension was applied to lacey carbon 300 mesh copper grids (Ted Pella), then blotted with Whatman #1 filter paper for 3 sec and vitrified in a Vitrobot Mark IV (FEI,Inc.). Similar experiment with native cardiac TFs yielded naked actin filaments decorated with C2.

Image analysis

Micrographs were collected with a 300-kV Titan Krios electron microscope equipped with a K3 direct electron with enabled energy filter and running in super resolution mode. Automatic data collection was performed with Leginon software. 3,315 micrographs were recorded in super resolution mode with 44 subframes with a dose rate of ~0.796 e-/$Å^2$ per frame over a defocus range of 0.6–3.5 μm with a pixel size of 0.54 Å. Motion correction and dose weighting was done using MotionCor2. Images were binned to 1.08 Å/px. The SPIDER software package [46] was used for image processing. Contrast transfer function parameters were calculated by using CTFFIND3 [47]. Particles were manually picked in EMAN2 e2helixboxer [48] and EMAN2 coordinates were used to extract 270,364 overlapping segments (300 pixels long). Fourier Shell Correlation was used to estimate the resolution.

3D-reconstruction of C2-decorated TFs

SPIDER software was used for the sorting and 3D reconstruction [46]. Three model volumes were created: pure F-actin (1), F-actin fully decorated with C2 (2), F-actin partially decorated with C2 (3) (PDB: 5K6P residues 358–451). These volumes were low-pass filtered to 26 Å, scaled to 2.16 Å per pixel and projected onto 150 × 150 px images with an azimuthal rotational increment of 4°, generating 270 reference projections (3 × 90). The C2-decorated TF segments were down-sampled to 2.16 Å per pixel and cross-correlated with 270 reference projections. Segments of images that had the best correlation with the pure F-actin model (n=115,145) and partially decorated with C2 (n=112,172) were excluded from further sorting, while the remaining structural class of segments containing fully decorated C2 segments (n=43,047) were reconstructed with the IHRSR method [49] starting from the solid cylinder as a starting model.

Segments assigned to the fully occupied C2 class (Figure S1(d)) were reconstructed at a raster of 1.08 Å and yielded a symmetry of −166.5°/27.31 Å. The final volume was corrected for the CTF by using a Wiener filter assuming that the signal-to-noise ratio in the volume was very large. Negative B-factor of 350 was used to amplify high frequencies in the reconstruction that were damped by the envelope function of the microscope. Based on the match between the high resolution structure of C2 domain (PDB: 5K6P residues 358–451) and cryo-EM density map (Fig. S2), the map was filtered to 7.5 Å resolution. Detailed statistics for the cryo-EM reconstruction is provided in Table S1.

Model building:

The cryo-EM density map served as a template for building an atomic model. UCSF Chimera map segmentation tool was used to extract six actin subunits, six C2 domains from the 7.5 Å resolution map (Fig. 2(a))The model of cardiac actin from the cardiac actomyosin complex (PDB: 7JH7) was docked into the density map as rigid body using UCSF Chimera [50]. The NMR structure of the human cardiac C2 domain (PDB: 5K6P) was truncated (residues 315–357 comprising the M-domain and the linker region were removed), and the structure of the C2 domain (residues 358–451) was manually docked into the density map using UCSF Chimera and subsequently refined with PHENIX software [51]. Statistical analysis of the atomic model is provided in Table S1.

ACCESSION NUMBERS

The atomic model has been deposited at the Protein Data Bank (www.rcsb.org) with accession code 7LRG. The corresponding cryo-EM map was deposited in the Electron Microscopy Data Bank (www.ebi.ac.uk/pdbe/emdb) with accession code EMD- 23497.

Supplementary Material

Refer to Web version on PubMed Central for supplementary material.

Acknowledgments:

This work was supported by R01 HL140925 (VEG, HDW and SPH), U24 GM116790 (VEG), and U24 GM116788 (VEG).

REFERENCES

[1]. Semsarian C, Ingles J, Maron MS, Maron BJ. New perspectives on the prevalence of hypertrophic cardiomyopathy. J Am Coll Cardiol. 2015;65:1249–54. [PubMed: 25814232]

[2]. Kensler RW, Craig R, Moss RL. Phosphorylation of cardiac myosin binding protein C releases myosin heads from the surface of cardiac thick filaments. Proc Natl Acad Sci U S A. 2017;114:E1355–E64. [PubMed: 28167762]

[3]. McNamara JW, Li A, Smith NJ, Lal S, Graham RM, Kooiker KB, et al.Ablation of cardiac myosin binding protein-C disrupts the super-relaxed state of myosin in murine cardiomyocytes. J Mol Cell Cardiol. 2016;94:65–71. [PubMed: 27021517]

[4]. Schmid M, Toepfer CN. Cardiac myosin super relaxation (SRX): a perspective on fundamental biology, human disease and therapeutics. Biol Open. 2021;10.

[5]. Hooijman P, Stewart MA, Cooke R. A new state of cardiac myosin with very slow ATP turnover: a potential cardioprotective mechanism in the heart. Biophys J. 2011;100:1969–76. [PubMed: 21504733]

[6]. McNamara JW, Singh RR, Sadayappan S. Cardiac myosin binding protein-C phosphorylation regulates the super-relaxed state of myosin. Proc Natl Acad Sci U S A. 2019;116:11731–6. [PubMed: 31142654]

[7]. McNamara JW, Li A, Lal S, Bos JM, Harris SP, van der Velden J, et al.MYBPC3 mutations are associated with a reduced super-relaxed state in patients with hypertrophic cardiomyopathy. PLoS One. 2017;12:e0180064. [PubMed: 28658286]

[8]. Belknap B, Harris SP, White HD. Modulation of thin filament activation of myosin ATP hydrolysis by N-terminal domains of cardiac myosin binding protein-C. Biochemistry. 2014;53:6717–24. [PubMed: 25265574]

[9]. Razumova MV, Bezold KL, Tu AY, Regnier M, Harris SP. Contribution of the myosin binding protein C motif to functional effects in permeabilized rat trabeculae. J Gen Physiol. 2008;132:575–85. [PubMed: 18955596]

[10]. Harris SP, Belknap B, Van Sciver RE, White HD, Galkin VE. C0 and C1 N-terminal Ig domains of myosin binding protein C exert different effects on thin filament activation. Proc Natl Acad Sci U S A. 2016;113:1558–63. [PubMed: 26831109]

[11]. Bezold KL, Shaffer JF, Khosa JK, Hoye ER, Harris SP. A gain-of-function mutation in the M-domain of cardiac myosin-binding protein-C increases binding to actin. J Biol Chem. 2013;288:21496–505. [PubMed: 23782699]

[12]. van Dijk SJ, Kooiker KB, Napierski NC, Touma KD, Mazzalupo S, Harris SP. Point mutations in the tri-helix bundle of the M-domain of cardiac myosin binding protein-C influence systolic duration and delay cardiac relaxation. J Mol Cell Cardiol. 2018;119:116–24. [PubMed: 29729251]

[13]. Luther PK, Winkler H, Taylor K, Zoghbi ME, Craig R, Padron R, et al.Direct visualization of myosin-binding protein C bridging myosin and actin filaments in intact muscle. Proc Natl Acad Sci U S A. 2011;108:11423–8. [PubMed: 21705660]

[14]. Rahmanseresht S, Lee KH, O'Leary TS, McNamara JW, Sadayappan S, Robbins J, et al.The N terminus of myosin-binding protein C extends toward actin filaments in intact cardiac muscle. J Gen Physiol. 2021;153.

[15]. Brunello E, Fusi L, Ghisleni A, Park-Holohan SJ, Ovejero JG, Narayanan T, et al.Myosin filament-based regulation of the dynamics of contraction in heart muscle. Proc Natl Acad Sci U S A. 2020;117:8177–86. [PubMed: 32220962]

[16]. Howarth JW, Ramisetti S, Nolan K, Sadayappan S, Rosevear PR. Structural insight into unique cardiac myosin-binding protein-C motif: a partially folded domain. J Biol Chem. 2012;287:8254–62. [PubMed: 22235120]

[17]. Jia W, Shaffer JF, Harris SP, Leary JA. Identification of novel protein kinase A phosphorylation sites in the M-domain of human and murine cardiac myosin binding protein-C using mass spectrometry analysis. J Proteome Res. 2010;9:1843–53. [PubMed: 20151718]

[18]. Gautel M, Zuffardi O, Freiburg A, Labeit S. Phosphorylation switches specific for the cardiac isoform of myosin binding protein-C: a modulator of cardiac contraction?EMBO J. 1995;14:1952–60. [PubMed: 7744002]

[19]. Ponnam S, Sevrieva I, Sun YB, Irving M, Kampourakis T. Site-specific phosphorylation of myosin binding protein-C coordinates thin and thick filament activation in cardiac muscle. Proc Natl Acad Sci U S A. 2019;116:15485–94. [PubMed: 31308242]

[20]. Whitten AE, Jeffries CM, Harris SP, Trewhella J. Cardiac myosin-binding protein C decorates F-actin: implications for cardiac function. Proc Natl Acad Sci U S A. 2008;105:18360–5. [PubMed: 19011110]

[21]. Mun JY, Previs MJ, Yu HY, Gulick J, Tobacman LS, Beck PS, et al.Myosin-binding protein C displaces tropomyosin to activate cardiac thin filaments and governs their speed by an independent mechanism. Proc Natl Acad Sci U S A. 2014;111:2170–5. [PubMed: 24477690]

[22]. Inchingolo AV, Previs SB, Previs MJ, Warshaw DM, Kad NM. Revealing the mechanism of how cardiac myosin-binding protein C N-terminal fragments sensitize thin filaments for myosin binding. Proc Natl Acad Sci U S A. 2019;116:6828–35. [PubMed: 30877248]

[23]. Orlova A, Galkin VE, Jeffries CM, Egelman EH, Trewhella J. The N-terminal domains of myosin binding protein C can bind polymorphically to F-actin. J Mol Biol. 2011;412:379–86. [PubMed: 21821050]

[24]. Risi C, Belknap B, Forgacs-Lonart E, Harris SP, Schroder GF, White HD, et al.N-Terminal Domains of Cardiac Myosin Binding Protein C Cooperatively Activate the Thin Filament. Structure. 2018;26:1604–11. [PubMed: 30270174]

[25]. Shaffer JF, Wong P, Bezold KL, Harris SP. Functional differences between the N-terminal domains of mouse and human myosin binding protein-C. J Biomed Biotechnol. 2010;2010:789798. [PubMed: 20379391]

[26]. Mun JY, Gulick J, Robbins J, Woodhead J, Lehman W, Craig R. Electron microscopy and 3D reconstruction of F-actin decorated with cardiac myosin-binding protein C (cMyBP-C). J Mol Biol. 2011;410:214–25. [PubMed: 21601575]

[27]. Kunst G, Kress KR, Gruen M, Uttenweiler D, Gautel M, Fink RH. Myosin binding protein C, a phosphorylation-dependent force regulator in muscle that controls the attachment of myosin heads by its interaction with myosin S2. Circ Res. 2000;86:51–8. [PubMed: 10625305]

[28]. Herron TJ, Rostkova E, Kunst G, Chaturvedi R, Gautel M, Kentish JC. Activation of myocardial contraction by the N-terminal domains of myosin binding protein-C. Circ Res. 2006;98:1290–8. [PubMed: 16614305]

[29]. Razumova MV, Shaffer JF, Tu AY, Flint GV, Regnier M, Harris SP. Effects of the N-terminal domains of myosin binding protein-C in an in vitro motility assay: Evidence for long-lived cross-bridges. J Biol Chem. 2006;281:35846–54. [PubMed: 17012744]

[30]. Shaffer JF, Kensler RW, Harris SP. The myosin-binding protein C motif binds to F-actin in a phosphorylation-sensitive manner. J Biol Chem. 2009;284:12318–27. [PubMed: 19269976]

[31]. Ratti J, Rostkova E, Gautel M, Pfuhl M. Structure and interactions of myosin-binding protein C domain C0: cardiac-specific regulation of myosin at its neck?J Biol Chem. 2011;286:12650–8. [PubMed: 21297165]

[32]. Ababou A, Rostkova E, Mistry S, Le Masurier C, Gautel M, Pfuhl M. Myosin binding protein C positioned to play a key role in regulation of muscle contraction: structure and interactions of domain C1. J Mol Biol. 2008;384:615–30. [PubMed: 18926831]

[33]. Ababou A, Gautel M, Pfuhl M. Dissecting the N-terminal myosin binding site of human cardiac myosin-binding protein C. Structure and myosin binding of domain C2. J Biol Chem. 2007;282:9204–15. [PubMed: 17192269]

[34]. Previs MJ, Mun JY, Michalek AJ, Previs SB, Gulick J, Robbins J, et al.Phosphorylation and calcium antagonistically tune myosin-binding protein C's structure and function. Proc Natl Acad Sci U S A. 2016;113:3239–44. [PubMed: 26908872]

[35]. Colson BA, Thompson AR, Espinoza-Fonseca LM, Thomas DD. Site-directed spectroscopy of cardiac myosin-binding protein C reveals effects of phosphorylation on protein structural dynamics. Proc Natl Acad Sci U S A. 2016;113:3233–8. [PubMed: 26908877]

[36]. Gruen M, Prinz H, Gautel M. cAPK-phosphorylation controls the interaction of the regulatory domain of cardiac myosin binding protein C with myosin-S2 in an on-off fashion. FEBS Lett. 1999;453:254–9. [PubMed: 10405155]

[37]. Yamada Y, Namba K, Fujii T. Cardiac muscle thin filament structures reveal calcium regulatory mechanism. Nat Commun. 2020;11:153. [PubMed: 31919429]

[38]. Lin BL, Li A, Mun JY, Previs MJ, Previs SB, Campbell SG, et al.Skeletal myosin binding protein-C isoforms regulate thin filament activity in a Ca(2+)-dependent manner. Sci Rep. 2018;8:2604. [PubMed: 29422607]

[39]. Shaffer JF, Harris SP. Species-specific differences in the Pro-Ala rich region of cardiac myosin binding protein-C. J Muscle Res Cell Motil. 2009;30:303–6. [PubMed: 20217194]

[40]. Gimona M, Mital R. The single CH domain of calponin is neither sufficient nor necessary for F-actin binding. J Cell Sci. 1998;111:1813–21. [PubMed: 9625744]

[41]. Galkin VE, Orlova A, Fattoum A, Walsh MP, Egelman EH. The CH-domain of calponin does not determine the modes of calponin binding to F-actin. J Mol Biol. 2006;359:478–85. [PubMed: 16626733]

[42]. Galkin VE, Orlova A, Cherepanova O, Lebart MC, Egelman EH. High-resolution cryo-EM structure of the F-actin-fimbrin/plastin ABD2 complex. Proc Natl Acad Sci U S A. 2008;105:1494–8. [PubMed: 18234857]

[43]. Harris SP. Making waves: A proposed new role for myosin-binding protein C in regulating oscillatory contractions in vertebrate striated muscle. J Gen Physiol. 2021;153.

[44]. Siemankowski RF, White HD. Kinetics of the interaction between actin, ADP, and cardiac myosin-S1. J Biol Chem. 1984;259:5045–53. [PubMed: 6715335]

[45]. Spudich JA, Huxley HE, Finch JT. Regulation of skeletal muscle contraction. II. Structural studies of the interaction of the tropomyosin-troponin complex with actin. J Mol Biol. 1972;72:619–32. [PubMed: 4349760]

[46]. Frank J, Shimkin B, Dowse H. SPIDER - A modular software system for electron image processing. Ultramicroscopy. 1981;6:343–58.

[47]. Mindell JA, Grigorieff N. Accurate determination of local defocus and specimen tilt in electron microscopy. J Struct Biol. 2003;142:334–47. [PubMed: 12781660]

[48]. Tang G, Peng L, Baldwin PR, Mann DS, Jiang W, Rees I, et al.EMAN2: an extensible image processing suite for electron microscopy. J Struct Biol. 2007;157:38–46. [PubMed: 16859925]

[49]. Egelman EH. A robust algorithm for the reconstruction of helical filaments using single-particle methods. Ultramicroscopy. 2000;85:225–34. [PubMed: 11125866]

[50]. Pettersen EF, Goddard TD, Huang CC, Couch GS, Greenblatt DM, Meng EC, et al.UCSF Chimera--a visualization system for exploratory research and analysis. J Comput Chem. 2004;25:1605–12. [PubMed: 15264254]

[51]. Liebschner D, Afonine PV, Baker ML, Bunkoczi G, Chen VB, Croll TI, et al.Macromolecular structure determination using X-rays, neutrons and electrons: recent developments in Phenix. Acta Crystallogr D Struct Biol. 2019;75:861–77. [PubMed: 31588918]

Highlights:

- In contrast to C0 and C1, C2 binds to F-actin in one structural mode
- C2 does not activate the thin filament
- Residues of C0, C1 and C2 involved in interaction with actin are not conserved

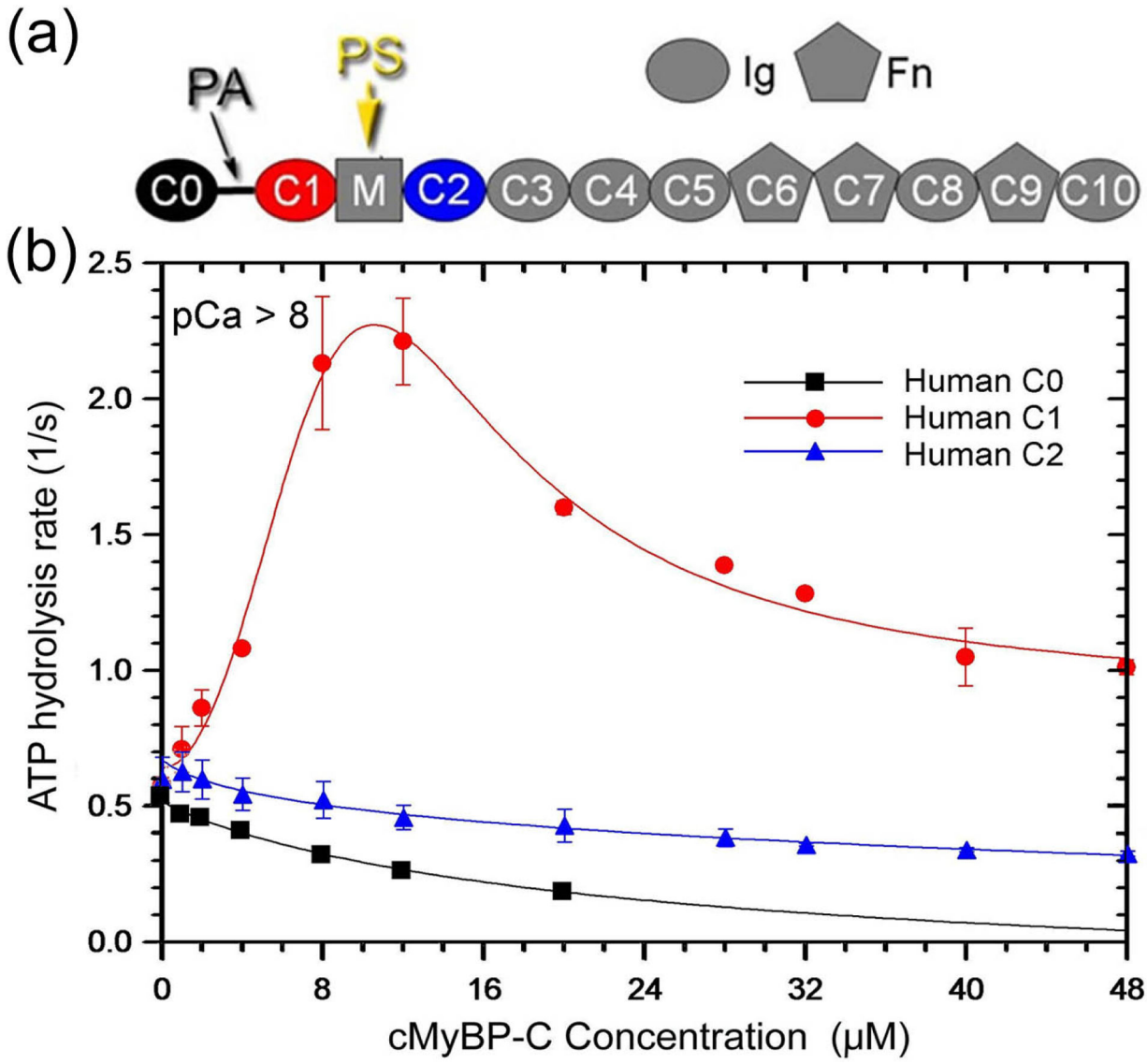

Figure 1. Effects of Individual N-terminal domains C0, C1 and C2 on TF-activated myosin-S1 ATPase activity.

(a) cMyBP-C is comprised of eight immunoglobulin (Ig)-like and three fibronectin (Fn)-like domains numbered C0 to C10 starting consecutively from the N terminus to the C terminus of the molecule. C0 and C1 domains are connected with the proline/alanine (PA) linker. The M-domain contains phosphorylation sites (PS). **(b)** Data for C0 and C1 are replotted from [10]. For C0 data were fit by a simple inhibition equation $V(C0) = Vo/(1+ ([C0]/K_{iC0}))$, where $K_{iC0} = 12.1 \pm 1$ μM and $Vo = 0.6 \pm 0.1 \cdot s^{-1}$ is the ATPase rate in the absence of C protein domains. As reported previously [10], C1 shows cooperative activation and inhibition that yields a best fit using $V(C1) = V_1/(1 + (K_1/[C1])^n + ([C1]/K_i)^n) + V_o$ equation, where $V_1 = 3.2 \pm 0.3\ s^{-1}$, $K_m = 8.4 \pm 1$ μM, $K_i = 15.2 \pm 3$ μM, $n = 2.1 \pm 0.3$ and $V_o = 0.6 \pm 0.1 \cdot s^{-1}$. Experimental conditions were 10 mM mops, 50 mM KAc, 2 mM $MgCl_2$, 3 mM EGTA (pCa > 8), pH 7.0, 0.65 μM A1S1, 5 μM TFs and the indicated concentration of the N terminal domain subunits of cardiac myosin binding protein C. In the presence

of C2 the ATP hydrolysis rate was only partially inhibited at saturating C2 and was fit by $V(C2) = V_{C2}/(1+ ([C2]/K_{iC2})) + V_0$ where $V_{C2} = 0.40\ s^{-1} \pm 0.1 \cdot s^{-1}$, $K_{C2} = 10 \pm 2\ \mu M$ and $V_0 = 0.25 \pm 05\ s^{-1}$ is the rate when saturating C2 is bound. Error bars represent SEM.

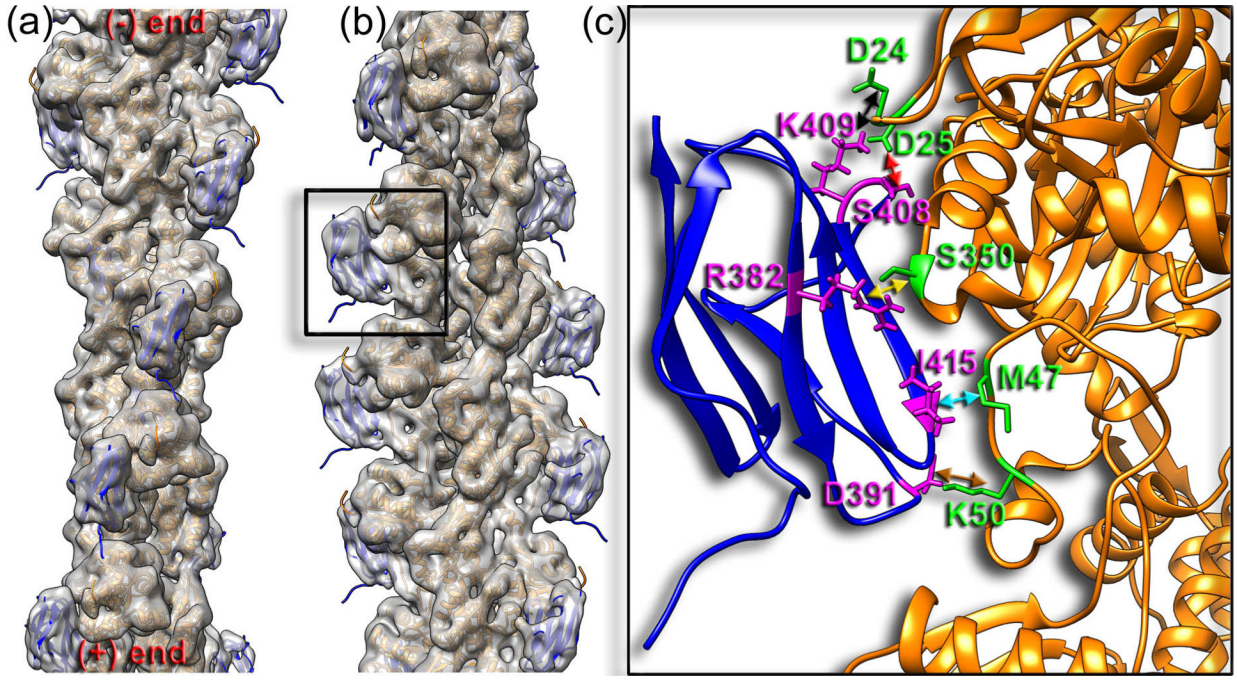

Figure 2. C2-decorated F-actin reconstruction.

(a) Density map (grey transparent surface) of C2 decorated F-actin at 7.5 Å resolution with the corresponding pseudo-atomic model comprised of actin (orange) and C2 (blue) molecules. The black box outlines the part of the model detailed in **(b)**. **(b)** Proposed interactions between C2 residues (magenta) and actin residues (green) that hold C2 on the surface of the actin filament are discussed in the text. The polarity of the actin filament is marked in red in (a).

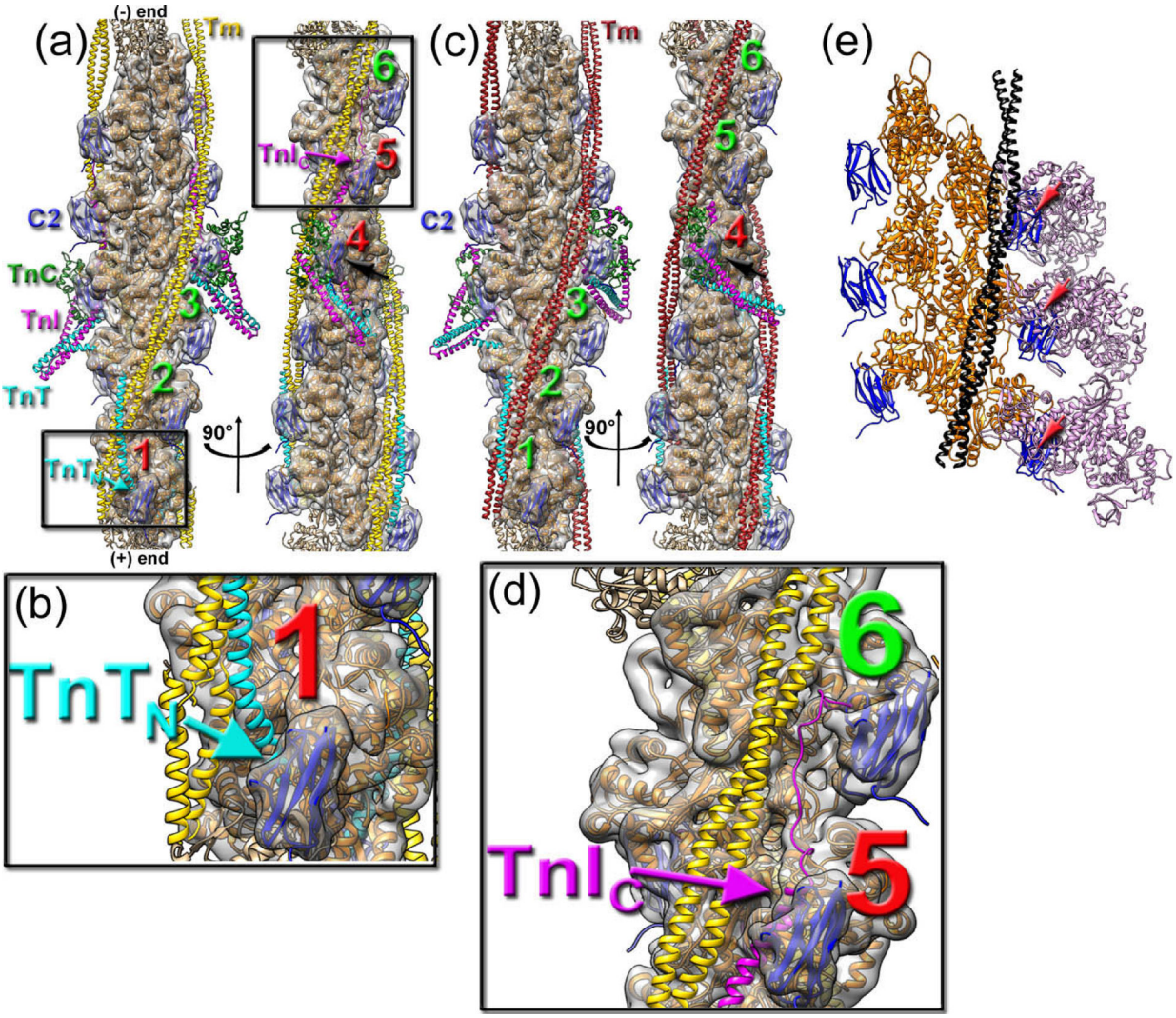

Figure 3. C2 binding sites projected on the surface of Ca^{2+}-free and Ca^{2+}-bound cardiac TF.

(a and **c)** The model of cardiac TF in **(a)** Ca^{2+}-free state (PDB: 6KN7) or **(c)** Ca^{2+}-bound state (PDB: 6KN8) was superimposed onto the C2-F-actin pseudo-atomic model shown in Figure 2 and the corresponding C2-F-actin map (grey transparent surface). The two views of the superimposed models and the map are related by 90° azimuthal rotation. Actin is show as orange ribbons, Tm is gold in (a) and brown in (c), TnC is green, TnI in magenta, TnT is cyan, while the C2 domain is shown in blue. Six actin subunits that comprise the regulatory unit on either actin strand are marked in numbers: the numbers of actins that are available for C2 interactions are in green, while inhibited actins are in red. The spatial clash of C2 with the core of the Tn complex at subunit 4 is marked with black arrows. **(b)** Detailed view of subunit 1 of cardiac TF in Ca^{2+}-free state shows a clash between TnT_N and C2 (cyan arrow). **(d)** Detailed view of subunits 5 and 6 of cardiac TF in Ca^{2+}-free state shows a clash between TnI_C and C2 (magenta arrow). **(e)** Superimposition of the cardiac actomyosin complex (PDB: 7JH7) onto the C2-F-actin model reveals major sterical clashes between the myosin head and C2 domain (red arrows, myosin is plum). The polarity of the actin filament is marked in black in (a).

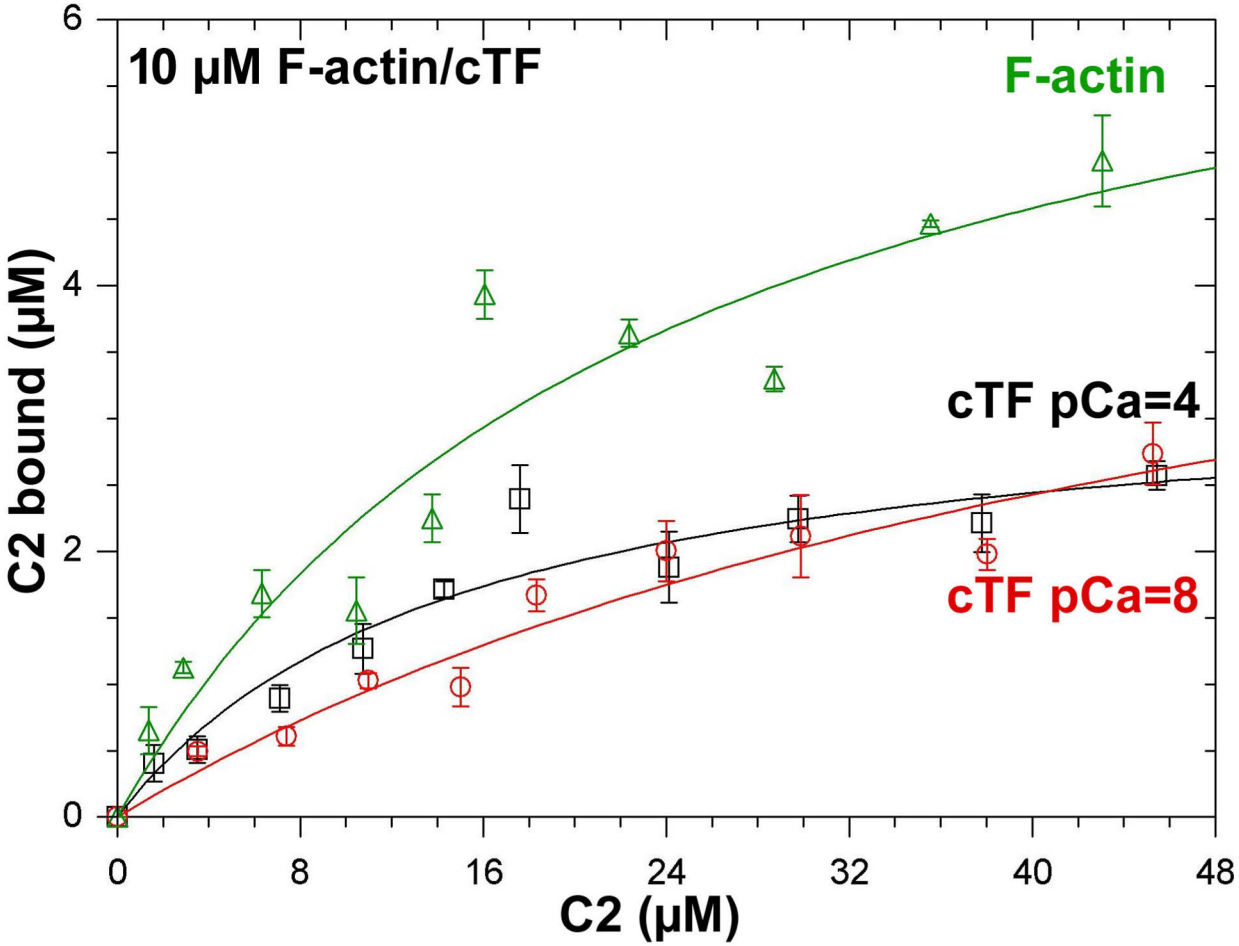

Figure 4. Binding of cMyBP-C C2 domain to F-actin and c-TF.

Comparison of C2 binding curves obtained using 10 uM of F-actin (green curve) or cTF at pCa=8 (red curve) and pCa=4 (black curve) shows that C2 binds to F-actin better than to the cTF, while preferentially binds to the Ca^{2+}-bound cTF. Data for C2 bound to F-actin were fit by $N_{FA}(C2) = N_{FAC2}/(1+(Kd_{FAC2}/[C2]))$ where Kd_{FAC2} = 24.0 +/− 7.6 μM and N_{FAC2} = 7.3 +/− 1.4 μM. Data for C2 bound to cTF at pCa=4 were fit by $N_{TF4}(C2) = N_{TF4C2}/(1+(Kd_{TF4C2}/[C2]))$ where Kd_{TF4C2} = 14.8 +/− 7.5 μM and N_{TF4C2} = 3.3 +/− 0.7 μM. Data for C2 bound to cTF at pCa=8 were fit by $N_{TF8}(C2) = N_{TF8C2}/(1+(Kd_{TF8C2}/[C2]))$ where Kd_{TF8C2} = 56.4 +/− 45.4 μM and N_{TF8C2} = 5.8 +/− 3.1 μM. Experimental conditions: 10 μM TF, 50 mM KAc, 10 mM MOPS, 1 mM EGTA, 3 mM $MgCl_2$, pH 7.0, 20° C. Error bars represent SEM.

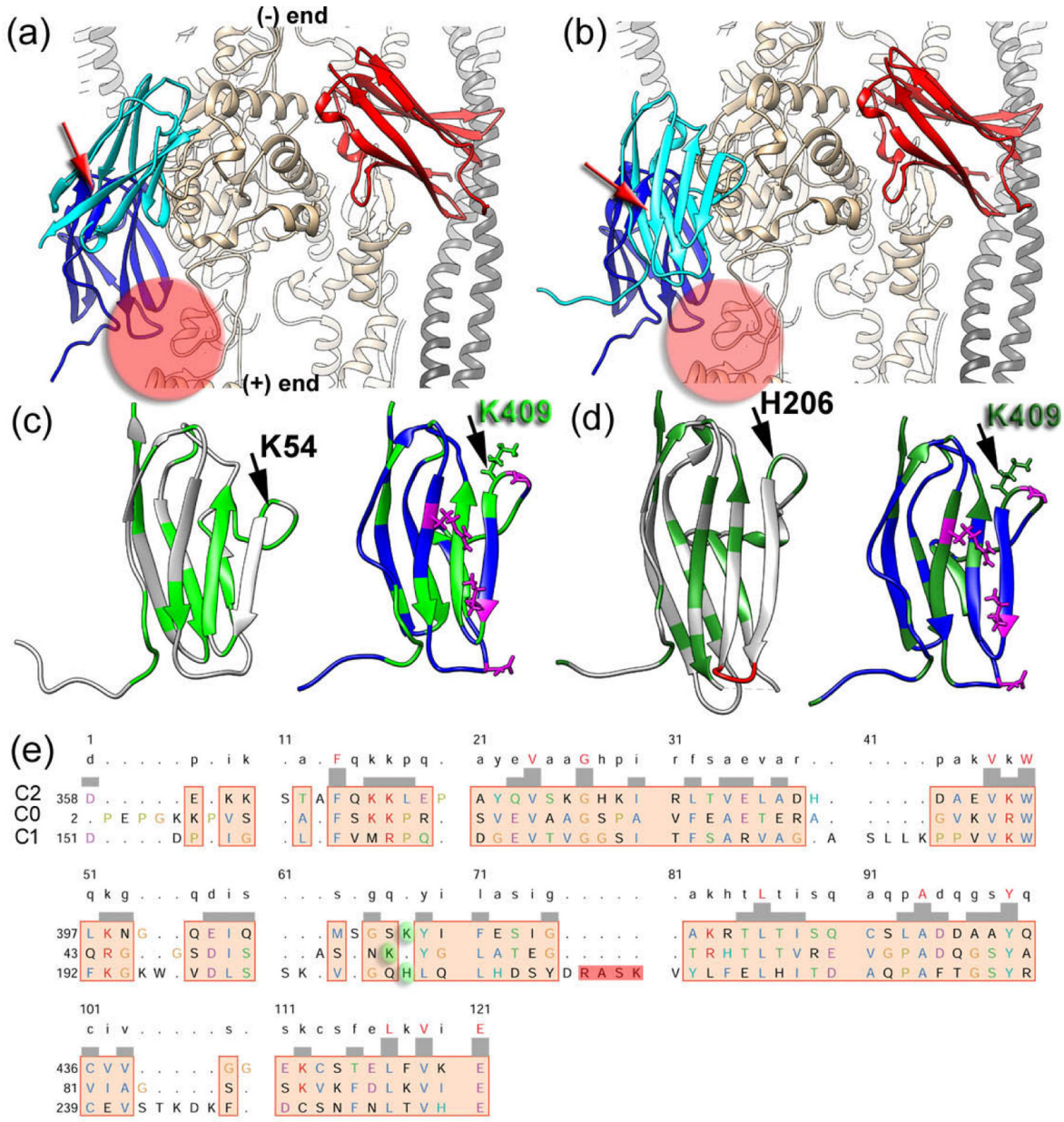

Figure 5. Comparison of C2 amino acid residues involved in interactions with F-actin with corresponding amino acid residues in C0 and C1.

(a and b) Atomic models of the two modes of C0–C1 bound to the TF where C0 is bound in either mode 1 (a) or mode 2 (b) show C0 in cyan, C1 in red, actin in tan and tropomyosin in dark grey. The position of C2 bound to F-actin is superimposed on these models with C2 shown in blue. C2 contact with the lower actin subunit is marked with red circle, while the spatial clash between C0 and C2 in either mode of C0 is depicted with red arrows. (c) High resolution structures of C0 (grey) and C2 (blue) have conserved amino acids marked in green. Side chains of residues of C2 involved in binding to F-actin are shown in magenta for non-conserved amino acids, while the only conserved lysine is outlined with black arrows in C0 (K54) and C2 (K409). (d) High resolution structures of C1 (grey) and C2 (blue) have conserved amino acids marked in dark green. Side chains of residues of C2 involved

in binding to F-actin are shown in magenta for non-conserved amino acids, while the only conserved amino acid is outlined with black arrows in C1 (H206) and C2 (K409). The RASK loop involved in the TF activation (red ribbons) [24] is absent in C2. (e) Amino acid sequence alignment of C2 with C0 and C1. The polarity of the actin filament is marked in black in (a).

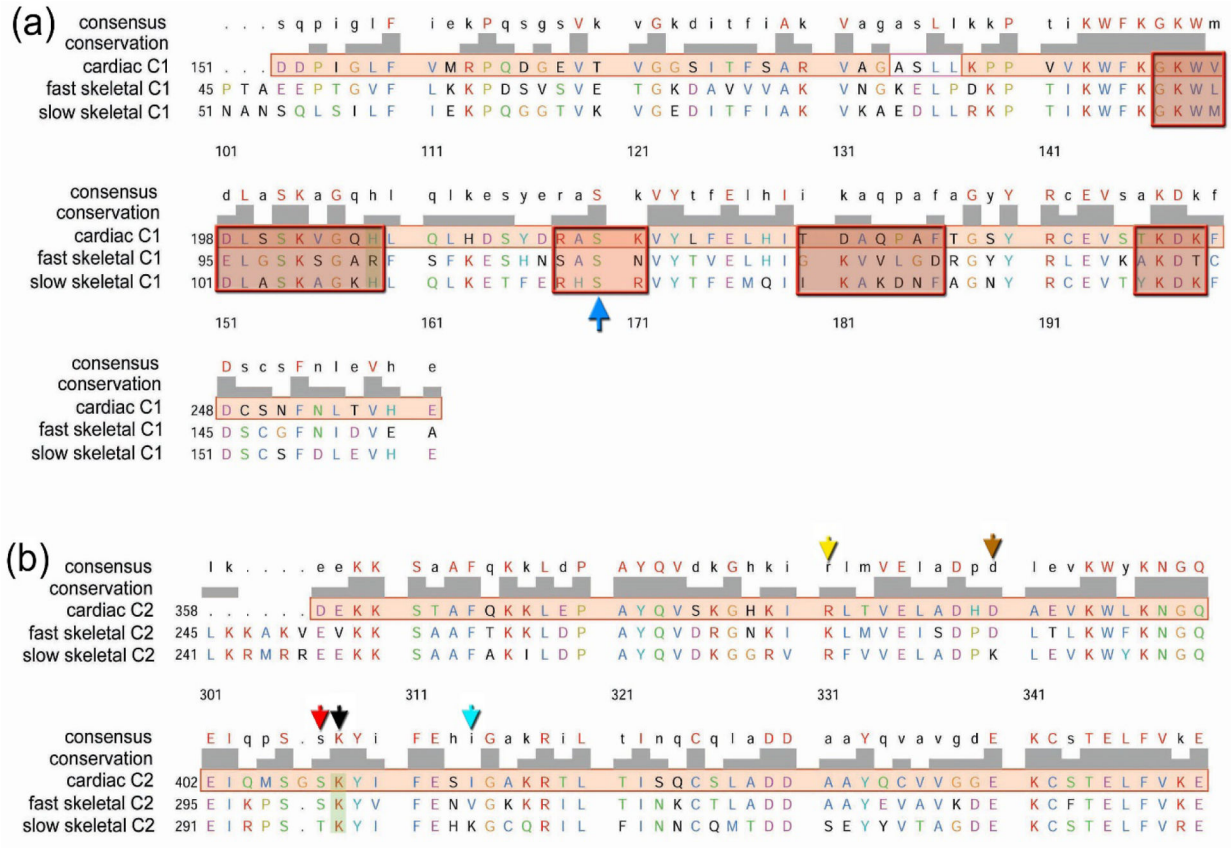

Figure 6. Comparison of cardiac C1 and C2 amino acid residues involved in interactions with the TF with corresponding amino acid residues in skeletal C1 and C2 isoforms.

(a) Amino acid sequence alignment of cardiac C1 with fast and slow skeletal isoforms. Residues predicted to be involved with F-actin interactions [10] are outlined in red boxes. The RASK loop involved in the cardiac TF activation [24] is marked with blue arrow. (b) Amino acid sequence alignment of cardiac C2 with fast skeletal and slow skeletal isoforms. Cardiac C2 residues involved in the interactions with F-actin are marked with arrows as follows: R382 is yellow, D391 is brown, S408 is red K409 is black, and I415 is cyan.